Geochemical Perspectives Letters

Oxygen minimum zones in the early Cambrian ocean

R. Guilbaud[1,2*], B.J. Slater[2,3], S.W. Poulton[4], T.H.P. Harvey[5], J.J. Brocks[6], B.J. Nettersheim[6,7], N.J. Butterfield[2]

OPEN ACCESS

doi: 10.7185/geochemlet.1806

Abstract

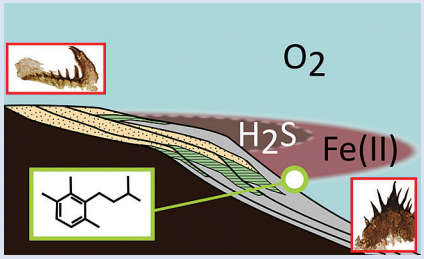

The relationship between the evolution of early animal communities and oceanic oxygen levels remains unclear. In particular, uncertainty persists in reconstructions of redox conditions during the pivotal early Cambrian (541-510 million years ago, Ma), where conflicting datasets from deeper marine settings suggest either ocean anoxia or fully oxygenated conditions. By coupling geochemical palaeoredox proxies with a record of organic-walled fossils from exceptionally well-defined successions of the early Cambrian Baltic Basin, we provide evidence for the early establishment of modern-type oxygen minimum zones (OMZs). Both inner- and outer-shelf environments were pervasively oxygenated, whereas mid-depth settings were characterised by spatially oscillating anoxia. As such, conflicting redox signatures recovered from individual sites most likely derive from sampling bias, whereby anoxic conditions represent mid-shelf environments with higher productivity. This picture of a spatially restricted anoxic wedge contrasts with prevailing models of globally stratified oceans, offering a more nuanced and realistic account of the Proterozoic-Phanerozoic ocean transition.

Received 18 September 2017 | Accepted 7 February 2018 | Published 1 March 2018

Introduction

The dramatically increased diversity of metazoan life through the late Ediacaran to early Cambrian transition (~585-510 Ma) coincides with a protracted transition from global ocean anoxia to widespread ocean oxygenation (Canfield *et al.*, 2007; Chen *et al.*, 2015; Von Strandmann *et al.*, 2015; Li *et al.*, 2017). Throughout the Proterozoic Eon (2500 to 541 Ma), the ocean is thought to have been characterised by oxygenated surface waters overlying euxinic (anoxic and sulphidic) mid-depth waters along productive ocean margins (Poulton *et al.*, 2010), and ferruginous (anoxic, Fe-containing) deeper waters (Planavsky *et al.*, 2011; Poulton and Canfield, 2011). Models for later Neoproterozoic oceans (635 to 541 Ma) also envisage redox stratification, with oscillations from strict anoxia to fully oxic conditions (Canfield *et al.*, 2007, 2008; Wood *et al.*, 2015). This dynamic ocean stratification is assumed to have persisted until the mid-Cambrian (Gill *et al.*, 2011; Chen *et al.*, 2015), by which time many key metazoan innovations had evolved.

Animals are fundamentally aerobic organisms - albeit with hugely varying oxygen demands - and their early fossil record is accordingly limited to oxygenated settings (Tostevin *et al.*, 2016). Most current models linking early animal evolution to redox chemistry assume a horizontally stratified ocean (Wood *et al.*, 2015; Jin *et al.*, 2016). However, modern oceans exhibit a marked lateral redox variability, most notably where combinations of high primary productivity and metazoan activity (Bianchi *et al.*, 2013) give rise to wedge-shaped oxygen minimum zones (Sperling *et al.*, 2015a). Determining which of these two models, horizontal or lateral, best characterises the structure of early Palaeozoic oceans is challenged by a dearth of spatial and temporal resolution, compounded by the removal of off-shelf signals due to subduction. Here, we exploit exceptionally well-preserved successions from the Baltic Basin to derive a high resolution redox model of early to middle Cambrian shelf seas (full details of geological setting and methods are provided as Supplementary Information).

Stratigraphy and Depositional Environments

We examined marine sediments from eight drill cores (Finngrundet-1, Bårstad-2, Bernstorp-1, Hamnudden-1, Böda Hamn-1, File Haidar-1, Grötlingbo-1 and Kostovo-13) spanning an area of 400 by 600 km across the Baltic Basin (Fig. 1). Studied sediments encompass the Lontova, File Haidar and Borgholm formations, deposited between the early Cambrian

1. Lancaster Environment Centre, Lancaster University, Lancaster LA1 4YQ, UK
2. Department of Earth Sciences, University of Cambridge, Cambridge CB2 3EQ, UK
* Corresponding author (email: r.guilbaud@cantab.net)
3. Department of Earth Sciences, Paleobiology, Uppsala University, 75236 Uppsala, Sweden
4. School of Earth and Environment, University of Leeds, Leeds LS2 9JT, UK
5. Department of Geology, University of Leicester, Leicester LE1 7RH, UK
6. Research School of Earth Sciences, The Australian National University, ACT 2601, Australia
7. Max Planck Institute for Biogeochemistry, Hans-Knoell-Strasse 10, 07745 Jena, Germany

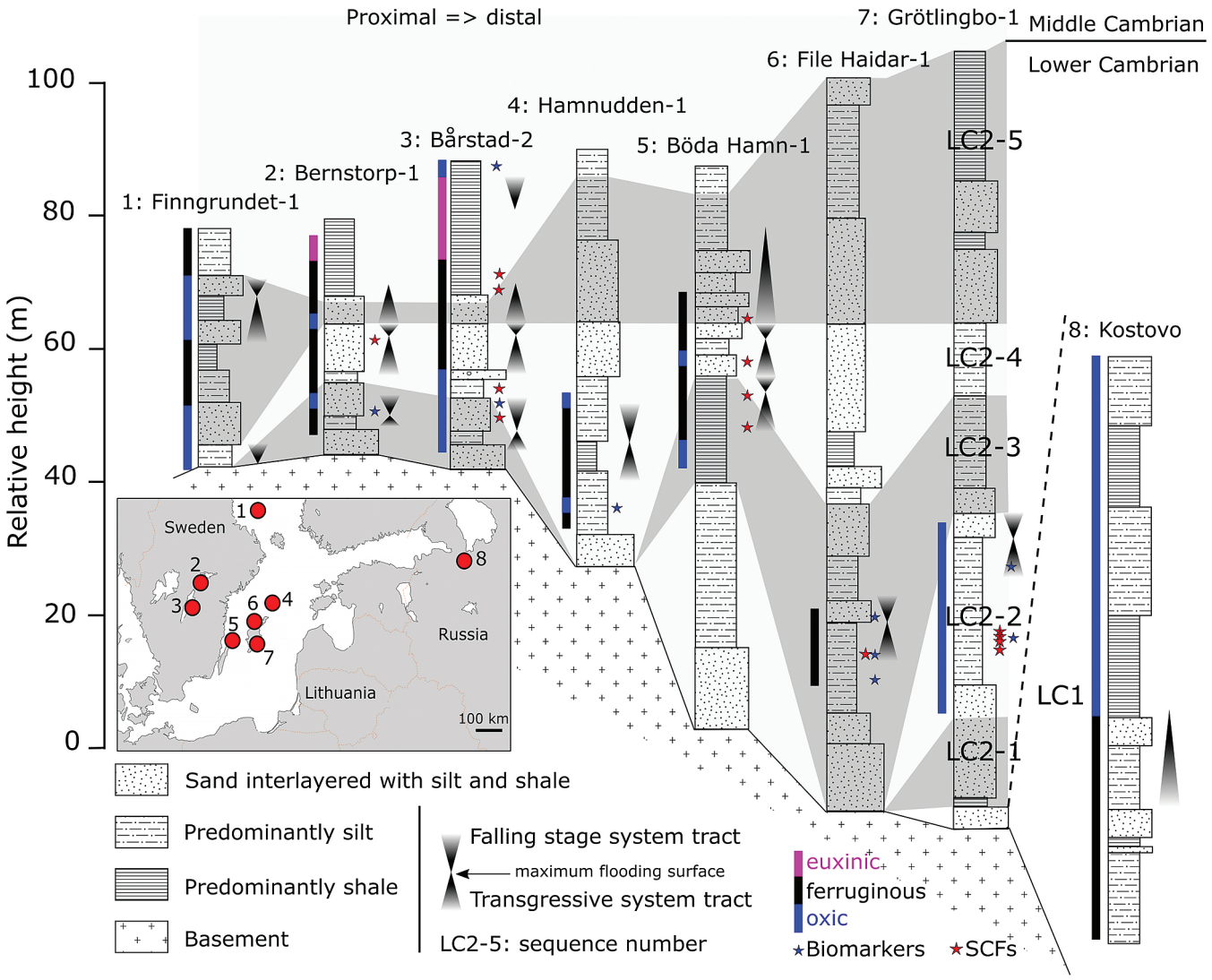

Figure 1 Core location (red circles) and stratigraphy, modified after Nielsen and Schovsbo (2011). Grey and white shadings represent the stratigraphic sequences (*e.g.*, LC2-5). The bars illustrate the analysed core sections (on mudstones and siltstones only); euxinic, ferruginous and oxic depositions are in purple, black and blue, respectively.

Fortunian stage and middle Cambrian Stage 5, and the internal stratigraphy and depositional environments of these siliciclastic sediments has been studied extensively (Hagenfeldt, 1994; Nielsen and Schovsbo, 2011, 2015). The studied area records a partial, yet substantial archive of contiguous sequences, organised into two supersequences for the lower Cambrian, 'LC1' and 'LC2', and one supersequence for the lower middle Cambrian, 'MC3' (Fig. 1). Nielsen and Schovsbo (2011, 2015) reconstructed the depositional environment of stratigraphic successions, reporting a gradient from proximal inner-shelf to mid-shelf and outer-shelf deposition below storm wave base. Inner-shelf deposition is recognised in all cores by abundant cross-bedding features within siltstones and generally coarser lithologies accompanying falling stage system tracts (FSSTs). Mid-shelf deposition is expressed as green silts and black shales with common glauconitic horizons and silty distal storm beds. Outer-shelf deposition is recognised by the presence of laminated mudstones and bioturbated siltstones in the absence of current features.

Results

Dominant water column redox conditions were determined *via* iron (Fe) speciation and trace metal systematics on mudstones and silts. Fe speciation relies on the quantification of highly reactive Fe (Fe_{HR}) relative to total Fe (Fe_T). Anoxic settings promote the formation of authigenic Fe minerals in the water column, resulting in Fe_{HR} enrichments in underlying sediments, with typically $Fe_{HR}/Fe_T \geq 0.38$ (Poulton and Canfield, 2011). By contrast, sediments deposited under oxic water columns lack Fe_{HR} enrichments, with $Fe_{HR}/Fe_T < 0.22$. Ratios between 0.22-0.38 are equivocal, and may represent either anoxic or oxic conditions, due to partial transformation of Fe_{HR} to sheet silicates during burial. We used Fe_T/Al enrichments (≥0.6) to evaluate this mechanism in instances of equivocal Fe_{HR}/Fe_T, since the ratio remains unaffected by diagenesis (Lyons and Severmann, 2006). For anoxic samples, ferruginous conditions are distinguished from euxinic settings by quantifying the extent of sulphidation of Fe_{HR}, whereby $Fe_P/Fe_{HR} \geq 0.7$ is characteristic of euxinic deposition and $Fe_P/Fe_{HR} < 0.7$ indicates ferruginous conditions (Poulton and Canfield, 2011).

Of the eight cores analysed, seven show marked stratigraphic shifts between oxic and anoxic deposition (Fig. 2). High concentrations of total organic carbon (TOC, up to ~20 %) are associated with anoxic conditions, reflecting enhancedorganic carbon preservation and supply, with the latter exerting a primary control on the development of anoxia. LC1 records dominantly anoxic conditions at the base of

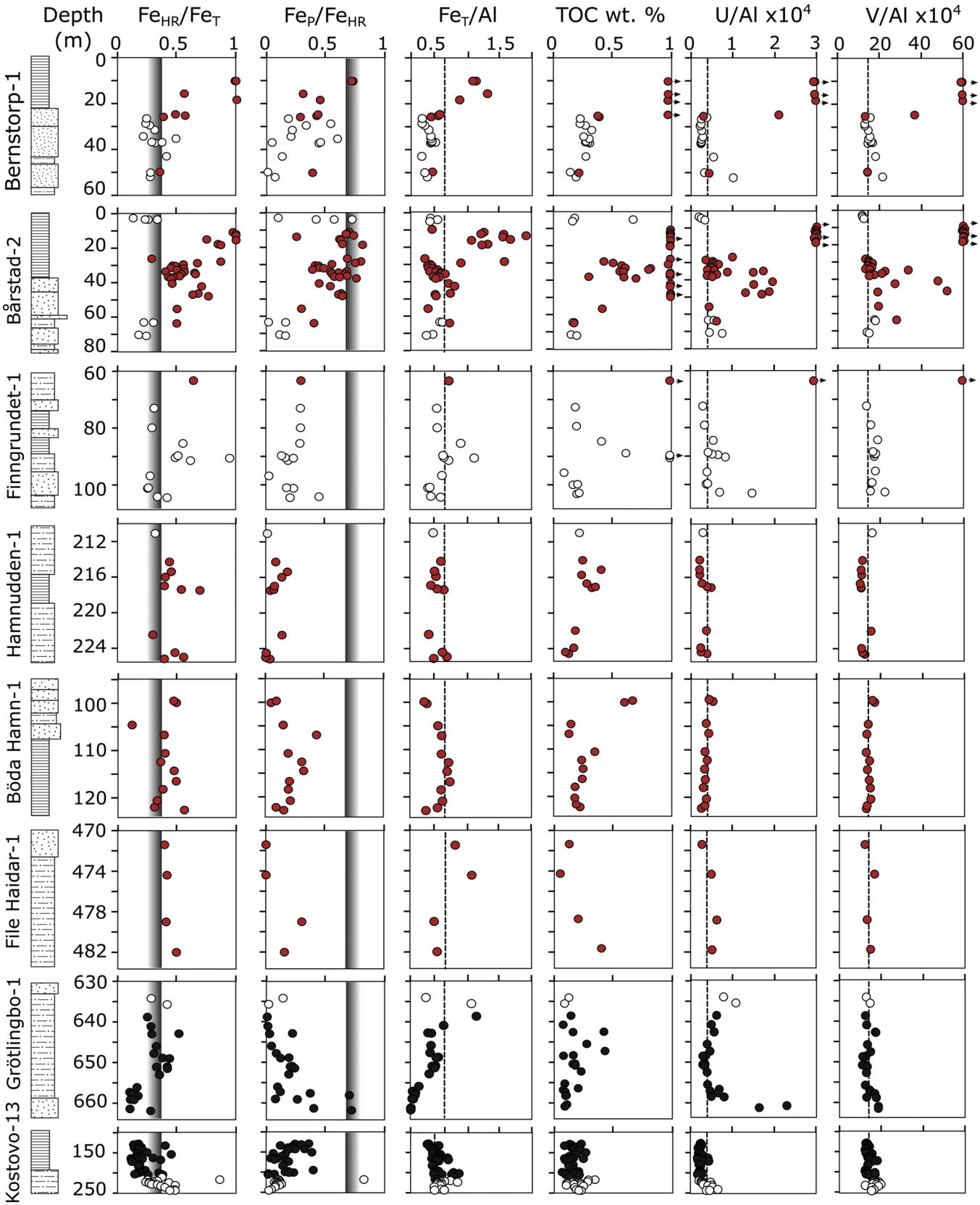

Figure 2 Geochemical data. Inner-, mid-, and outer-shelf environments are indicated by open, red and black symbols, respectively. Grey shadows delimit redox domains and dashed lines represent average shale values. Black arrows are for outpassing data points. Maximum values for U/Al and V/Al are 54 and 434 ppm/wt. %, respectively.

Kostovo-13, whereas oxic conditions prevail in the upper part of the core. Through LC2 and MC3, water column conditions are characterised predominately by ferruginous anoxia, with some euxinic horizons towards the top of Bårstad-2 and Bernstorp-1. Within these latter strata, oxic conditions prevail at the base of Grötlingbo-1 and throughout all FSSTs (Figs. 1 and 2).

Redox variations between sequences are likely to reflect temporal changes. Furthermore, the core availability did not permit us to track each sequence in their full lateral expression. Therefore, in order to integrate water column redox data into a palaeo-environmental framework, we used the reconstructions of shelf environments in the Baltic Basin (Nielsen

and Schovsbo 2011, 2015) as binning discriminants (Fig. 3a). This statistical approach allows us to build a time-independent model for the redox architecture of the basin. Throughout the deposition of all successions, we observe statistically significant differences in the redox chemistry of inner-, mid- and outer-shelf environments (Table S-2). Oxic conditions systematically dominate throughout FSSTs, inner- and outer-shelf settings. Anoxic conditions, by contrast, tend to prevail in mid-shelf environments. Such distribution strongly suggests that the shelf was largely oxygenated at this time, with an expansion of anoxia limited to mid-shelves (Fig. 4). Trace metal (U and V) variations support Fe_T/Al and Fe speciation data, with pronounced sedimentary enrichments under euxinic water column conditions (Fig. 2). We note that for some instances of apparent oxic deposition based on Fe speciation (*e.g.*, at the basal and uppermost parts of the Grötlingbo-1 core), U enrichments are coeval with muted V enrichments, indicating low-oxygen conditions (Zhang *et al.*, 2016), comparable to that seen in modern OMZs (see Supplementary Information for details).

We complemented the inorganic redox proxies with biomarker indicators selected from mid-shelf sediments (Finngrundet-1, Bårstad-2, Bernstorp-1). The ratio of pristane to phytane (Pr/Ph) is low (0.46-0.79), supporting a dominantly anoxic mid-depth water column (Schwark and Frimmel, 2004). In these anoxic environments, 2,3,6-trimethyl aryl isoprenoids (AI) likely derived from anaerobic phototrophic green sulphur bacteria (GSB), and their detection indicates that the water column was temporarily anoxic up to the photic zone (Brocks *et al.*, 2005). The ratio between shorter- (C_{13} to C_{17}) and longer-chain (C_{18} to C_{22}) AI (the AI ratio, AIR) is used as a measure of oxidative degradation during deposition (Schwark and Frimmel, 2004). Despite AI production in anoxic settings, the range and magnitude of AIR values (1.3 to 5.8) provide independent support for transient oxygenated conditions beneath the anoxic zone (Fig. 3b). Together with our Fe speciation data, this suggests that anoxic mid-depth waters overlaid oxygenated waters, enhancing oxidative degradation of AI during deposition.

Further evidence for distinct redox conditions across the shelf comes from the record of 'small carbonaceous fossils' (SCFs) (Butterfield and Harvey, 2012), found in oxic inner- and outer-shelf settings and ferruginous mid-shelf environments (Fig. 1). All recognisable SCFs are the remains of benthic aerobic animals, including *Wiwaxia*, stem-annelids, priapulids and palaeoscolecid worms (Fig. 3c). In contrast to sparsely fossiliferous mid-shelves, inner- and outer-shelf facies preserved most diverse SCFs assemblages, along with conspicuous burrows and bioturbation fabrics (Slater *et al.*, 2017). These palaeontological data corroborate the geochemical signatures for oxygenated inner- and outer-shelf environments (Fig. 3c). Fossilisation is of course a combination of both organismal ecology and taphonomic opportunity. Transient ferruginous conditions represent the dynamic interface between the oxic conditions where most metazoans live, and the anoxic conditions necessary to preserve non-biomineralising forms. Therefore, the apparently paradoxical persistence of SCFs in ferruginous settings may imply an iron shuttle from the core to the edges of the OMZ, enhancing the Fe_{HR} flux to oxygenated settings, or more likely dynamic oscillations between oxic and ferruginous water column conditions – in contrast to more permanently anoxic mid-shelves which were devoid of benthic metazoans and prone to euxinia.

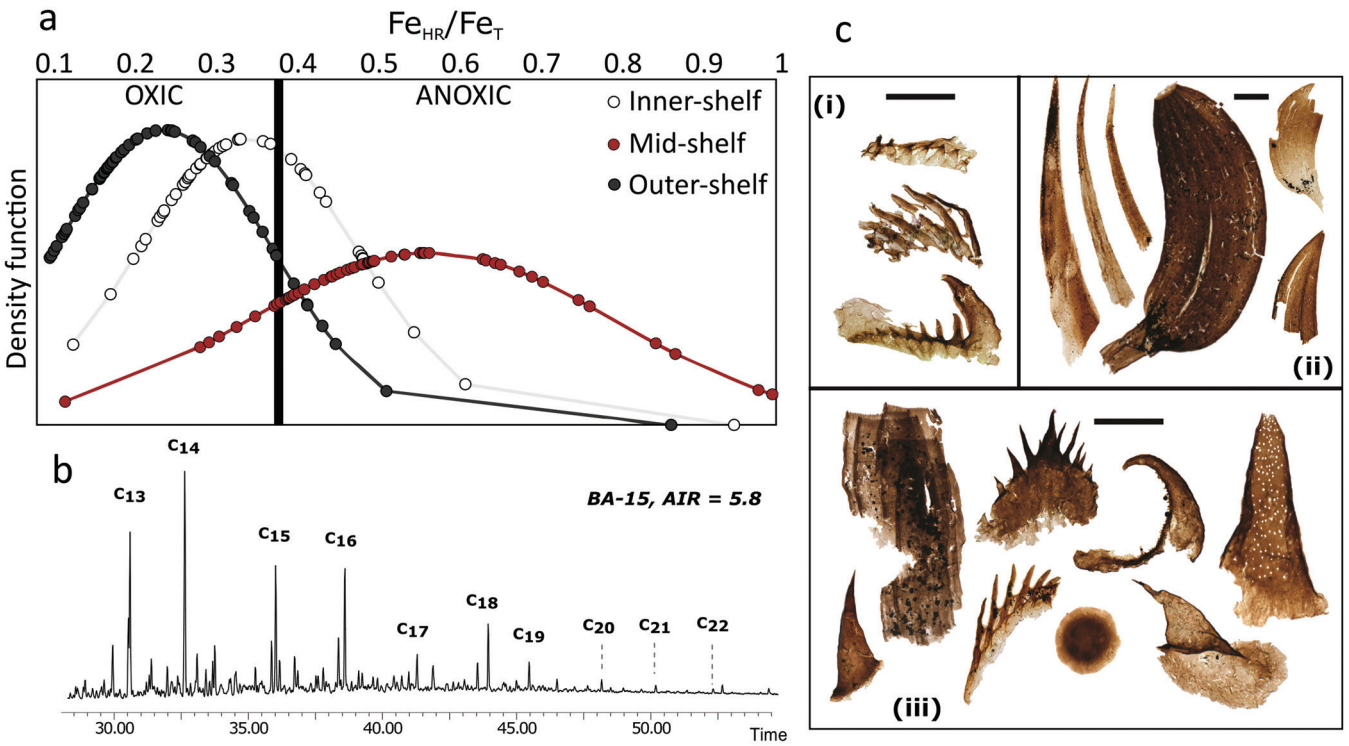

Figure 3 **(a)** Distribution of redox ratios (n = 183), binned as a function of their depositional environment. Inner- and outer-shelf environments show significantly more oxic redox populations than corresponding mid-shelves (t test $p << 0.05$). **(b)** Example of m/z = 134 partial ion chromatogram revealing the presence of 2,3,6 trimethyl aryl isoprenoids (AI) in mid-shelf facies. High ratios of short- to long-chain AI (AIR) point to strongly varying, intermittent oxygen exposure levels. **(c)** SCF assemblages from (i) inner-shelf (denticulate metazoan structures), (ii) mid-shelf (protoconodont spines alongside occasional *Wiwaxia* sclerites) and (iii) outer-shelf environments (priapulid, palaeoscolecid and annelid remains). Scale bars are 100 µm.

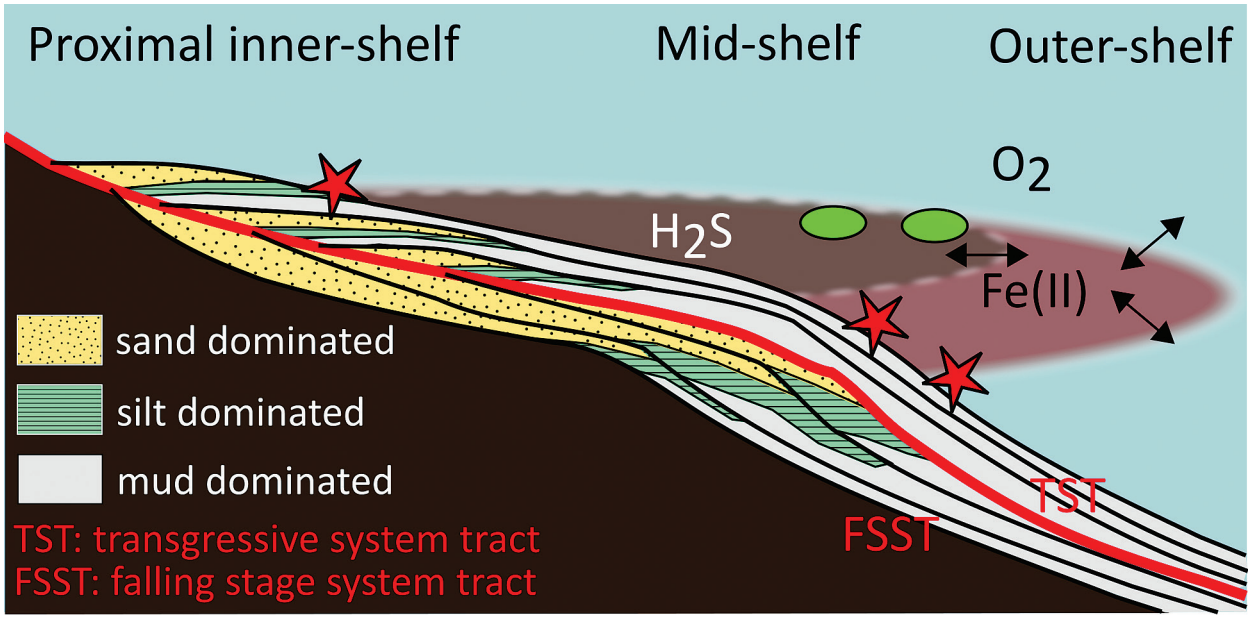

Figure 4 Redox architecture reconstruction, with oxic conditions above and below anoxic settings. Ferruginous conditions dominate in the OMZ, but euxinia develops in zones of increased organic carbon delivery. Metazoan body fossils recovery is shown by the red stars. Evidence for phototrophic GSB (green ovals) in mid-shelf settings corroborates geochemical and palaeontological redox indicators.

Implications

Our data provide evidence for a lateral expression of redox variation, which resembles the structure of modern OMZs (Fig. 4), although oxygen depletion was likely more pronounced and at shallower depths than in modern counterparts. Gentle topographical slope and reduced circulation in the relatively shallow Baltic Basin may have further exacerbated the role of benthic oxygen uptake, analogous to shallow OMZs (Brandt *et al.*, 2015). The discovery of OMZ denitrification in early Cambrian successions of China (Hammarlund *et al.*, 2017) suggests that our model may have been a common feature of contemporaneous margins. The record of ancient marine sedimentary rocks is certainly biased towards continental margins, which promotes the sampling of environments prone to host OMZs. Thus, in the absence of detailed spatial and temporal resolution, apparent horizontal stratification may often capture the upper boundary of OMZs, over-estimating global deep-water anoxia. By contrast, the recognition of such structure would explain the large discrepancies reported through the Neoproterozoic-Cambrian transition (*e.g.*, Sperling *et al.*, 2015b). Our data augments emerging views of early Cambrian expanded marine oxygenated conditions (Chen *et al.*, 2015; Li *et al.*, 2017), supporting the establishment of a modern-like ocean architecture during the 'explosion' of metazoan diversity (Butterfield, 2018).

Conclusion

Identification of dynamic wedge-shaped OMZs along the margins of the early Cambrian Baltic Basin raises the question of the antiquity of such structures. The evolutionary switch from a prokaryote- to eukaryote-dominated biological pump is thought to have played an essential role in the ventilation of the deep ocean (Butterfield, 2009, 2018; Lenton *et al.*, 2014). The subsequent establishment of modern-type OMZs, as identified in the early Cambrian ocean, may have developed as a consequence of contemporaneous metazoan expansion, whereby animal activity maintains high levels of oxygen depletion in OMZs (Bianchi *et al.*, 2013). However, OMZ structures may track back to older, Mesoproterozoic oceans (Zhang *et al.*, 2016). Although fundamental differences in pre-metazoan biological pump may have given terminal Proterozoic OMZs a distinct expression (presumably thicker and shallower), this overall geometry may have been a prevalent feature of late Precambrian oceans.

Acknowledgements

We are thankful to Linda Wickström (Geological Survey of Sweden), Ursula Toom, Olle Hints and Heikki Bauert (Tallinn University of Technology), and Tõnis Saadre (Estonian Geological Survey) for sampling support, and James Rolfe, Jason Day and Janet Hope for analytical technical support. The authors are thankful to the constructive comments of T. Lyons, C. Scott and an anonymous reviewer. This work was funded by NERC (NE/K005251/1). SWP acknowledges support from a Royal Society Wolfson Research Merit Award.

Editor: Liane G. Benning

Author contributions

RG, BJS, THPH and NJB collected samples. RG extracted and interpreted geochemical data with significant contributions from BJN, JJB and SWP. BJS extracted and interpreted palaeontological data with significant contributions from THPH and NJB. RG and BJS wrote the manuscript, with significant contributions from all co-authors.

Additional Information

Supplementary Information accompanies this letter at http://www.geochemicalperspectivesletters.org/article1806.

Cite this letter as: Guilbaud, R., Slater, B.J., Poulton, S.W., Harvey, T.H.P., Brocks, J.J., Nettersheim, B.J., Butterfield, N.J. (2018) Oxygen minimum zones in the early Cambrian ocean. *Geochem. Persp. Let.* 6, 33-38.

References

Bianchi, D., Galbraith, E.D., Carozza, D.A., Mislan, K.A.S., Stock, C.A. (2013) Intensification of open-ocean oxygen depletion by vertically migrating animals. *Nature Geoscience* 6, 545–548.

Brandt, P., Bange, H.W., Banyte, D., Dengler, M., Didwischus, S.-H., Fischer, T., Greatbatch, R.J., Hahn, J., Kanzow, T., Karstensen, J., Körtzinger, A., Krahmann, G., Schmidtko, S., Stramma, L., Tanhua, T., Visbeck, M. (2015) On the role of circulation and mixing in the ventilation of oxygen minimum zones with a focus on the eastern tropical North Atlantic. *Biogeosciences (BG)* 12, 489–512.

Brocks, J.J., Love, G.D., Summons, R.E., Knoll, A.H., Logan, G.A., Bowden, S.A. (2005) Biomarker evidence for green and purple sulphur bacteria in a stratified Palaeoproterozoic sea. *Nature* 437, 866–870.

Butterfield, N.J. (2009) Oxygen, animals and oceanic ventilation: an alternative view. *Geobiology* 7, 1–7.

Butterfield, N.J. (2018) Oxygen, animals and aquatic bioturbation: An updated account. *Geobiology* 16, 3–16.

Butterfield, N., Harvey, T. (2012) Small carbonaceous fossils (SCFs): a new measure of early Paleozoic paleobiology. *Geology* 40, 71–74.

Canfield, D.E., Poulton, S.W., Narbonne, G.M. (2007) Late-Neoproterozoic Deep-Ocean Oxygenation and the Rise of Animal Life. *Science* 315, 92–95.

Canfield, D.E., Poulton, S.W., Knoll, A.H., Narbonne, G.M., Ross, G., Goldberg, T., Strauss, H. (2008) Ferruginous Conditions Dominated Later Neoproterozoic Deep-Water Chemistry. *Science* 321, 949–952.

Chen, X., Ling, H.-F., Vance, D., Shields-Zhou, G.A., Zhu, M., Poulton, S.W., Och, L.M., Jiang, S.-Y., Li, D., Cremonese, L., Archer, C. (2015) Rise to modern levels of ocean oxygenation coincided with the Cambrian radiation of animals. *Nature Communications* 6, 7142.

Gill, B.C., Lyons, T.W., Young, S.A., Kump, L.R., Knoll, A.H., Saltzman, M.R. (2011) Geochemical evidence for widespread euxinia in the Later Cambrian ocean. *Nature* 469, 80–83.

Hagenfeldt, S.E. (1994) The Cambrian File Haidar and Borgholm Formations in the central Baltic and south central Sweden. *Stockholm Contributions in Geology* 43, 69–110.

Hammarlund, E.U., Gaines, R.R., Prokopenko, M.G., Qi, C., Hou, X.-G., Canfield, D.E. (2017) Early Cambrian oxygen minimum zone-like conditions at Chengjiang. *Earth and Planetary Science Letters* 475, 160–168.

Jin, C., Li, C., Algeo, T.J., Planavsky, N.J., Cui, H., Yang, X., Zhao, Y., Zhang, X., Xie, S. (2016) A highly redox-heterogeneous ocean in South China during the early Cambrian (~529–514 Ma): Implications for biota-environment co-evolution. *Earth and Planetary Science Letters* 441, 38–51.

Lenton, T.M., Boyle, R.A., Poulton, S.W., Shields-Zhou, G.A., Butterfield, N.J. (2014) Co-evolution of eukaryotes and ocean oxygenation in the Neoproterozoic era. *Nature Geoscience* 7, 257–265.

Li, C., Jin, C., Planavsky, N.J., Algeo, T.J., Cheng, M., Yang, X., Zhao, Y., Xie, S. (2017) Coupled oceanic oxygenation and metazoan diversification during the early–middle Cambrian? *Geology* 743–746.

Lyons, T.W., Severmann, S. (2006) A critical look at iron paleoredox proxies: new insights from modern euxinic marine basins. *Geochimica et Cosmochimica Acta* 70, 5698–5722.

Nielsen, A.T., Schovsbo, N.H. (2011) The Lower Cambrian of Scandinavia: depositional environment, sequence stratigraphy and palaeogeography. *Earth-Science Reviews* 107, 207–310.

Nielsen, A.T., Schovsbo, N.H. (2015) The regressive Early-Mid Cambrian 'Hawke Bay Event' in Baltoscandia: Epeirogenic uplift in concert with eustasy. *Earth-Science Reviews* 151, 288–350.

Planavsky, N.J., McGoldrick, P., Scott, C.T., Li, C., Reinhard, C.T., Kelly, A.E., Chu, X., Bekker, A., Love, G.D., Lyons, T.W. (2011) Widespread iron-rich conditions in the mid-Proterozoic ocean. *Nature* 477, 448–451.

Poulton, S.W., Canfield, D.E. (2011) Ferruginous Conditions: A Dominant Feature of the Ocean through Earth's History. *Elements* 7, 107–112.

Poulton, S.W., Fralick, P.W., Canfield, D.E. (2010) Spatial variability in oceanic redox structure 1.8 billion years ago. *Nature Geoscience* 3, 486–490.

Schwark, L., Frimmel, A. (2004) Chemostratigraphy of the Posidonia Black Shale, SW-Germany: II. Assessment of extent and persistence of photic-zone anoxia using aryl isoprenoid distributions. *Chemical Geology* 206, 231–248.

Slater, B.J., Harvey, T.H.P., Guilbaud, R., Butterfield, N.J. (2017) A cryptic record of Burgess Shale-type diversity from the early Cambrian of Baltica. *Palaeontology* 60, 117–140.

Sperling, E.A., Knoll, A.H., Girguis, P.R. (2015a) The Ecological Physiology of Earth's Second Oxygen Revolution. *Annual Review of Ecology, Evolution, and Systematics* 46, 215–235.

Sperling, E.A., Wolock, C.J., Morgan, A.S., Gill, B.C., Kunzmann, M., Halverson, G.P., Macdonald, F.A., Knoll, A.H., Johnston, D.T. (2015b) Statistical analysis of iron geochemical data suggests limited late Proterozoic oxygenation. *Nature* 523, 451–454.

Tostevin, R., Wood, R.A., Shields, G.A., Poulton, S.W., Guilbaud, R., Bowyer, F., Penny, A.M., He, T., Curtis, A., Hoffmann, K.H., Clarkson, M.O. (2016) Low-oxygen waters limited habitable space for early animals. *Nature Communications* 7, 12818.

Von Strandmann, P.A.P., Stüeken, E.E., Elliott, T., Poulton, S.W., Dehler, C.M., Canfield, D.E., Catling, D.C. (2015) Selenium isotope evidence for progressive oxidation of the Neoproterozoic biosphere. *Nature Communications* 6, 10157.

Wood, R.A., Poulton, S.W., Prave, A.R., Hoffmann, K.-H., Clarkson, M.O., Guilbaud, R., Lyne, J.W., Tostevin, R., Bowyer, F., Penny, A.M., Curtis, A., Kasemann, S.A. (2015) Dynamic redox conditions control late Ediacaran metazoan ecosystems in the Nama Group, Namibia. *Precambrian Research* 261, 252–271.

Zhang, S., Wang, X., Wang, H., Bjerrum, C.J., Hammarlund, E.U., Costa, M.M., Connelly, J.N., Zhang, B., Su, J., Canfield, D.E. (2016) Sufficient oxygen for animal respiration 1,400 million years ago. *Proceedings of the National Academy of Sciences* 113, 1731–1736.

Geochemical Perspectives Letters

Oxygen minimum zones in the early Cambrian ocean

R. Guilbaud, B.J. Slater, S.W. Poulton, T.H.P. Harvey, J.J. Brocks, B.J. Nettersheim, N.J. Butterfield

Supplementary Information

The Supplementary Information includes:

- Geological Descriptions
- Methods
- Trace Metal Geochemistry
- Biomarker Maturity and Redox Indicators
- Distribution of Redox Data through Depositional Environments
- Distribution of SCFs and Diversity
- Tables S-1 (Excel download) and S-2
- Figures S-1 to S-4
- Supplementary Information References

Geological Descriptions

Samples were collected from core material spanning over a large area of the Baltic basin (Fig. 1). The sedimentary successions have undergone little diagenesis (Kirsimäe *et al.*, 1999) and low thermal maturity (see below), which is ideal for a combined study of SCF preservation and geochemical proxies. During early-mid Cambrian times, Baltica formed an isolated paleo-continent (Kirschvink *et al.*, 1997). Cambrian sediments on Baltica, which consist of successions of siliciclastic sediments, ranging from coarse sands and siltstones to clay-dominated mudstones, were deposited in a shallow, pericratonic sea with an exceptionally gentle shelf slope (Nielsen and Schovsbo, 2011). Minor changes in eustatic sea levels could therefore flood large expanses of the Baltic shelf. The stratigraphy of early to middle Cambrian successions in the Baltic basin has been studied extensively (Hagenfeldt, 1989a,b, 1994; Schovsbo, 2001; Nielsen and Schovsbo, 2011, 2015). We have adopted herein the nomenclature by Nielsen and Schovsbo (Nielsen and Schovsbo, 2011, 2015), who assembled a comprehensive sequence stratigraphic framework for the Baltic Basin centred on major cycles of progradational deposition interrupted by pulses of marine transgression – recorded as recurring falling stage system tracts (FSST) and transgressive system tracts (TST) respectively. These stratigraphic sequences are themselves organised into higher, '2nd order' sequences (referred to as supersequences), separated by subaerial unconformities due to regional-scale regression events such as the Hawke Bay Event (Bergström and Ahlberg, 1981; Hagenfeldt and Bjerkéus, 1991; Nielsen and Schovsbo, 2011, 2015). In the studied area, the lower Cambrian includes two supersequences, 'LC1' and 'LC2' (Nielsen and Schovsbo, 2011), whereas the lower middle Cambrian is part of one supersequence, 'MC3' (Nielsen and Schovsbo, 2015). The western Baltic Basin records a partial, yet substantial archive of the LC1, LC2 and MC3 supersequences, and the studied cores provided stratigraphically well resolved samples for four of the five contiguous LC2 sequences (from LC2-2 to LC2-5), along with

single sequences from LC1 and MC3. Significantly, correlated LC2 strata were sampled across seven of the eight cores (Finngrundet-1, Bårstad-2, Bernstorp-1, Hamnudden-1, Böda Hamn-1, File Haidar-1 and Grötlingbo-1) allowing a high resolution accounting of the basin geometry.

Nielsen and Schovsbo (2011, 2015) reconstructed the depositional environment of stratigraphic successions at the time of maximum flooding, reporting a gradient from proximal inner-shelf to mid-shelf and outer-shelf deposition. The nomenclature used here is as follows: inner-shelf area corresponds to the sea floor deposited between the normal wave base and the storm wave base. Outer-shelf corresponds to the sea floor deposited below the storm wave base. The mid-shelf corresponds to the distal inner-shelf or/and proximal outer-shelf. Our earliest Cambrian samples ('LC1') comprise green-grey silts and mudstones from the Rovno and the Lontova formations (Kostovo-13 core). Rovno Formation sediments are dominated by silts with common cross-bedding features, and the lithology is generally coarser-grained than Lontova sediments. Inner-shelf and outer-shelf depositional environments have been interpreted for the Rovno and the Lontova formations, respectively (Nielsen and Schovsbo, 2011). The lower File Haidar Formation (Hagenfeldt, 1994) was sampled through the 'LC2-2' and 'LC2-3' sequences. The 'LC2-2' sequence recorded in the Grötlingbo-1 core consists of mudstone and bioturbated siltstones interpreted as outer-shelf sediments (Nielsen and Schovsbo, 2011), and siltstone layers within a dominantly sandy unit interpreted as FSST. Our samples from the 'LC2-3' sequence consists of fining upward bioturbated silts and sandstones recorded in the File Haidar-1 core, glauconitic silts from the Böda Hamn-1 core, and silt horizons within sand-dominated units in the Bårstad-2 and Bernstorp-1 cores. The generally coarser lithology of the File Haidar-1 core is suggestive of a more proximal environment on the paleo-shelf, relative to the Grötlingbo-1 core, and 'LC2-3' sediments from the Böda Hamn-1 core were also interpreted as distal inner-shelf (Nielsen and Schovsbo, 2011), while coarser sediments from the Bårstad-2 and Bernstorp-1 cores are suggested to represent the falling stage system tract of the sequence. Later lower Cambrian successions 'LC2-4' are recorded by the upper File Haidar Formation (Hagenfeldt, 1994) through mudstones and sands from the Hamnudden-1, Böda Hamn-1, Finngrundet-1, Bårstad-2 and Bernstorp-1 cores (Hagenfeldt, 1989a, 1994; Nielsen and Schovsbo, 2011). In the Hamnudden-1 core, 'LC2-4' sediments consist of unusually thick (relative to the other cores) bioturbated greenish silts and shaley horizons interpreted as proximal outer-shelf or distal inner-shelf sediments (Nielsen and Schovsbo, 2011), and medium- to fine-grained sandstone interpreted as FSST. In the Böda Hamn-1 core, the 'LC2-4' sequence is thinner but also consists of greenish silts. In the Finngrundet-1 core, the 'LC2-4' sequence is characterised by greenish clays and silts with sandy storm beds. The lithology is generally coarser than in the Hamnudden-1 core, indicative of inner-shelf deposition (Nielsen and Schovsbo, 2011). In the Bårstad-2 and Bernstorp-1 cores, 'LC2-4' silts are generally coarser and sands more common than in the Hamnudden core, suggesting a more proximal position on the paleo-slope (Nielsen and Schovsbo, 2011). Like the 'LC2-4' sequence, 'LC2-5' deposits are recorded through the upper File Haidar Formation (Hagenfeldt, 1994), from the Böda Hamn-1, Finngrundet-1, Bårstad-2 and Bernstorp-1 cores (Hagenfeldt, 1989a, 1994; Nielsen and Schovsbo, 2011). In the Finngrundet-1 core, our samples consist of black to greenish silts with occurrence of sandy storm beds, suggestive of inner-shelf deposition (Nielsen and Schovsbo, 2011), and the material is generally coarser than in the Böda Hamn-1 core. The 'LC2-5' sequence in the Bårstad-2 and Bernstorp-1 cores is marked by a sand-dominated coarser lithology, which we did not sample. Middle Cambrian successions are preserved throughout the Bårstad-2, Bernstorp-1 and Finngrundet-1 cores, and consist of laminated grey silts and grey to black shales (Thickpenny, 1984; Hagenfeldt, 1989b, 1994; Schovsbo, 2001; Nielsen and Schovsbo, 2015) with sandier storm beds, suggestive of proximal outer-shelf to distal inner-shelf deposition. Bioturbated, coarser grained silts at the base and the top of the sections are interpreted as inner-shelf deposition.

Methods

All data are reported in Table S-1. The iron speciation method was performed on powdered mudstones and silts horizons, or shaley interbeds within coarser deposits, following well-established Fe sequential extraction schemes (Poulton and Canfield, 2005) which target operationally defined Fe pools, including carbonate associated-Fe (FeCarb), ferric oxide-Fe (FeOx), magnetite-Fe (FeMag), pyrite-Fe (FeP) and total Fe (FeT). Highly reactive Fe (FeHR) is calculated as FeHR = FeCarb + FeOx+ FeMag + FeP. For each sample, FeCarb, FeOx, and FeMag. were extracted sequentially by a sodium acetate leach (48 hr at 50 °C), followed by a sodium dithionite leach (2 hr at ambient temperature) and an ammonium oxalate leach (6 hr at ambient temperature), respectively. Bulk sediments were digested by a HNO_3-HF-$HClO_4$-H_3BO_3-HCl dissolution. [Fe] in each extract and in the bulk digestion was measured by Atomic Absorption Spectroscopy and replicate analyses gave a RSD <4 % for each step, leading to <8 % for calculated FeHR, which is comparable to the precision obtained by other laboratories (Poulton and Canfield, 2005). Replicate analyses of representative shales (n = 10) gave a precision of ± 0.01 on both the FeHR/FeT and the FeP/FeHR ratios. The final fraction of FeHR, (FeP) was calculated from the wt. % of sulphide extracted as Ag_2S using hot Cr(II)Cl_2 distillation (Canfield *et al*., 1986). A boiling HCl distillation prior to the Cr(II)Cl_2 distillation ruled out the potential presence of acid volatile sulphides in our samples. Analysis of a certified reference material (PACS-2, FeT = 3.97 ± 0.06 wt. %, n = 5; certified value = 4.09 ± 0.06 wt. %) confirms the validity of our total Fe dissolution.

Al, V and U concentrations in total digestions were determined by ICP-MS and replicate analyses gave a RSD <4 % on representative shales (n = 10). Analysis of the PACS-2 certified standard (n = 5) indicates a 98 % recovery for Al, V and U, and 97 %

recovery for Fe, which confirms the validity of our total dissolution. U/Al and V/Al (ppm/wt. %) ratios have been used to track anoxic and suboxic basins through Earth's history (Partin *et al.*, 2013; Lyons *et al.*, 2014; Zhang *et al.*, 2016). Mobile U is removed from the water column under reducing conditions in association with organic matter (McManus *et al.*, 2005). Under low oxygen conditions, particulate U can persist when V is remobilised, resulting in authigenic U enrichments and muted V signals under low oxygen conditions.

TOC was determined as the difference between total carbon (TC) before and after inorganic carbon removal (two 25 % (vol/vol) HCl washes for 24 hours). Samples were analysed on a carbon analyser and replicate analyses gave a precision of ±0.09 wt. % (2σ level).

Biomarker syngeneity was ensured by employing the Exterior/Interior methodology described in detail elsewhere (Brocks *et al.*, 2008; Jarrett *et al.*, 2013). Briefly, hydrocarbon contaminants on exterior surfaces and in cracks of drill core samples were removed by micro-ablation of rock surfaces. Ablated, clean rock fragments ('interior') were crushed to powder using a steel puck mill, and the ablated rock slurry ('exterior') was dried at 40 °C. The powdered rock interiors and exteriors were extracted with dichloromethane : methanol (90:10 v/v) using a Dionex Accelerated Solvent Extractor. Extract volumes were reduced to ~100 µl under a gentle steam of N_2 and fractionated over dry-packed silica gel columns using 1.5 dead volumes (DV) of *n*-hexane for saturated hydrocarbons, 2 DV of *n*-hexane : dichloromethane (4:1 v/v) for aromatic hydrocarbons, and 2 DV of dichloromethane : methanol (1:1 v/v) for the polar fraction. Extracts were analysed by gas chromatography-mass spectrometry (GC-MS) on an Agilent 6890 GC, coupled to a Micromass Autospec Premier double sector MS using well established protocols (Jarrett *et al.*, 2013). Saturated and aromatic fractions were spiked with 18-methyl eicosanoic acid methyl ester (18-MEME, Chiron Laboratories AS) as internal standard. The micro-ablation technique successfully removed hydrocarbon contaminants from rock surfaces (Fig. S-1). All biomarker ratios cited in this study (Table S-1) are from clean interior fractions.

Samples were processed for SCFs using a low-manipulation HF maceration procedure (Butterfield, 1994). 50 grams of sediment per sample were digested and organic debris collected in deionised water. SCFs were pipette-picked and subsequently mounted on glass slides for study. The majority of identified metazoan fossils are sourced from demonstrably benthic metazoans (*Wiwaxia sp.*, stem-annelids, and priapulid and palaeoscolecid worms) and preserve an array of delicate cuticular features, lacking any signs of abrasion. These factors, in combination with the co-occurrence of SCFs with bioturbated horizons, suggest that these fossils were not subject to significant transportation, indeed the priapulids, palaeoscolecids and annelids were potentially sourced from the burrow producers.

Trace Metal Geochemistry

We considered the geochemical behaviour of uranium and vanadium (McManus *et al.*, 2006; Och and Shields-Zhou, 2012; Partin *et al.*, 2013; Zhang *et al.*, 2016) as a gauge for low-oxygen conditions. Under anoxic conditions ($Fe_{HR}/Fe_T > 0.38$), the reduction of soluble uranyl and vanadate species removes U and V from the water column and underlying sediments are typically enriched in both U and V (McManus *et al.*, 2006; Zhang *et al.*, 2016). Under oxic conditions ($Fe_{HR}/Fe_T < 0.38$), transport of U and V to the sediment are through complexation with organic matter and adsorption onto Mn oxides, and organic matter consumption and Mn oxide reduction in the sediment will release U and V back to the water column. When low levels of oxygen are present in the water column, vanadate escapes from the sediment whilst particulate U can persist, resulting in acute U enrichments but muted V signals in the sediment (Zhang *et al.*, 2016). Such a trace metal pattern is observed for our sediments where $Fe_{HR}/Fe_T < 0.38$, which suggests that low-oxygen zones were common above the sediment.

Biomarker Maturity and Redox Indicators

Phenanthrene (P) and methylphenanthrene (MP) peaks were measured on trace m/z 178+192, and the methylphenanthrene index (MPI) was calculated as MPI = 1.5 x [(3-MP) + (2-MP)]/[P + (1-MP) + (9-MP)]. Vitrinite reflectance equivalents (Rc) were calculated from the MPI (Boreham *et al.*, 1988) as: Rc = [0.7 x MPI] + 0.22. All three biomarker samples show similarly low Rc, indicating that organic and inorganic geochemical proxies are unlikely to be strongly affected by thermal maturity and deep burial processes.

Acyclic isoprenoids pristane (Pr, C_{19}) and phytane (Ph, C_{20}) were quantified in *m/z* 85 ion chromatograms. The degradation of (bacterio)chlorophyll-derived phytol under reducing conditions predominantly results in the production of phytane, whereas oxic conditions cause generation of pristane by loss of a terminal carbon atom through decarboxylation. Although variations in the biological source of acyclic isoprenoid precursors can influence the Pr/Ph ratio, it is generally regarded as an indicator for the exposure of senescent biomass to oxygen (Peters *et al.*, 2005). In the Baltic samples, Pr/Ph values range from 0.46 to 0.79 (Table S-1). Such Pr/Ph <1 are commonly explained by early diagenetic exposure of phytol to largely reducing conditions.

2,3,6-trimethyl aryl isoprenoids (AI) were quantified in *m/z* 134 ion chromatograms of the aromatic fractions (Fig. S-2). Compounds were identified by comparison with elution positions and mass spectra of the external standard B03162eA from the

1.64 billion years old Barney Creek Formation (Brocks *et al.*, 2005). Although 2,3,6-trimethyl AI may form by degradation of carotenoids with the β-carotane skeleton (Koopmans *et al.*, 1996), in environments with an anoxic water column, such as the Black Sea, they are typically derived from aromatic carotenoids of obligatory anaerobic phototrophic green sulphur bacteria (Chlorobiaceae) (Summons and Powell, 1987; Brocks and Schaeffer, 2008). Thus, the presence of these markers usually indicates that the water column was (transiently) anoxic up into the photic zone of the water column. The aryl isoprenoid ratio (AIR), which measures the relative abundance of short- (C_{13} to C_{17}) and longer-chain (C_{18} to C_{22}) AI, is an indicator for the degradation of carotenoids through oxygen exposure (Schwark and Frimmel, 2004). As the precursor organisms inhabit the anoxic photic zone, such degradation must occur as the dead biomass sinks through deeper oxygenated waters or is exposed to oxygen at the sediment-water interface prior to permanent burial. Thus, the range and magnitude of values in the mid-shelf environment of the Baltic basin (AIR = 1.3 to 5.8) indicate variations in the exposure to oxygen before permanent burial. This is consistent with a fluctuating anoxic wedge.

Distribution of Redox Data through Depositional Environments

Redox data were binned into three depositional environmental types, as in inner-shelf, mid-shelf, and outer-shelf throughout the entire successions from the early to mid-Cambrian. Depositional environments of transgression system tracts were determined by the environments of maximum flooding surfaces (Nielsen and Schovsbo, 2011), which correspond to the deeper archive of the given environment. This diminishes the effect of relative water depth variations within each sequence, and allows a time-independent redox reconstruction of shelf environments in a systematic and conservative manner. Because falling stage system tracts correspond to the shallowest settings of a given depositional environment, redox data from FSST were binned as 'inner-shelf' environments. Student's t-tests (Table S-2) for unequal variances suggest that the populations of the three depositional environments are statistically different (absolute t-stat > t-critical and $p \ll 0.05$). We also explored the density functions of redox data binned against additional parameters (Fig. S-4), such as the relative position of sections on the palaeo-slope (referred to here as 'section-binning procedure'), and geological formations (referred to here as 'formation-binning procedure'), as both could, to a certain extent, be considered as palaeo-slope indicators (Nielsen and Schovsbo, 2011).

Distribution of SCFs and Diversity

Evidence for metazoans in the form of SCFs and trace fossils shows significant partitioning between inner- mid- and outer-shelf sediments (Fig. 3c). Among sediments of the inner-shelf, finer grained lithologies yield abundant and diverse SCFs (see also Slater *et al.*, 2017). Given the predominance of coarser sandstones in these proximal environments, the total abundance of SCFs is lower than that recorded among outer-shelf strata. However, these shallow marine sandstones (*e.g.*, the Mickwitzia Sandstone Member) record an abundance and exceptionally diverse range of trace fossils, betraying the presence of a rich benthic fauna (Jensen, 1997). Palynological processing of mid-shelf sediments typically recovers only amorphous organic matter, also reflected by the higher TOC contents (Fig. 2), and general paucity of SCFs. Occasional horizons contain numerous protoconodonts, though these are likely sourced from surface-water dwelling chaetognaths, and so do not reflect benthic conditions. Rare sclerites of Wiwaxia are also recovered from mid-shelf sediments (Fig. 3c). Wiwaxiids were certainly benthic, however, their preservation in a broad spectrum of environments (from mud-cracked emergent sediments to relatively deeper marine Lagerstätten settings) points to a remarkably broad ecophysiological tolerance and a general recalcitrance and transportability of their scalids, which are frequently found in sediments devoid of other SCFs. The richest diversity and highest abundance of SCFs are preserved in sediments of the outer-shelf (Slater *et al.*, 2017). Like their inner-shelf counterparts, these outboard sediments show numerous signs of bioturbation and an active infauna.

Supplementary Tables

Table S-1 All geochemical data (both organic and inorganic).

Table S-1 is available for download as an Excel file at http://www.geochemicalperspectivesletters.org/article1806.

Table S-2 t-tests for the redox populations of inner-, mid- and outer-shelfs.

	t-test 1		t-test 2	
	Inner-shelf	Outer-shelf	Inner-shelf	Mid-shelf
Mean	0.349	0.246	0.350	0.575
Variance	0.018	0.017	0.018	0.051
Observations	49	61	49	64
Hypothesised Mean Difference	0		0	
Df	102		106	
t Stat	4.0458		-6.5853	
P(T<=t) one-tail	5.08E-05		8.96E-10	
t Critical one-tail	1.6599		1.6594	
t Critical two-tail	1.9835		1.9826	

Supplementary Figures

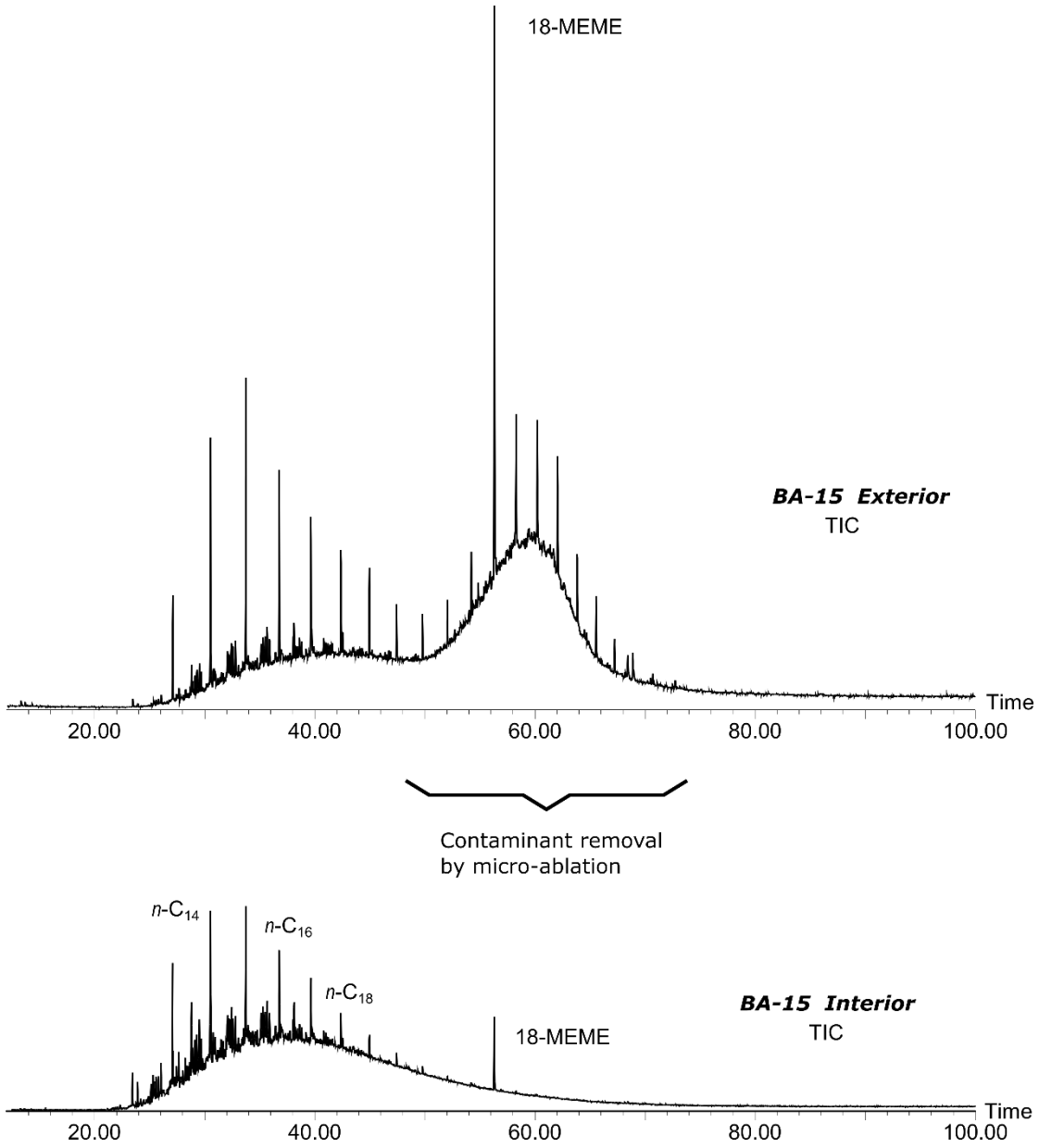

Figure S-1 Total ion chromatograms (TIC) of the saturated hydrocarbon fraction of BA-15 illustrating the removal of higher molecular weight organic molecules (>50 min elution) from contaminated rock surfaces and cracks during the micro-ablation procedure. 18-MEME is the internal standard, *n*-C_x are *n*-alkanes with carbon number x.

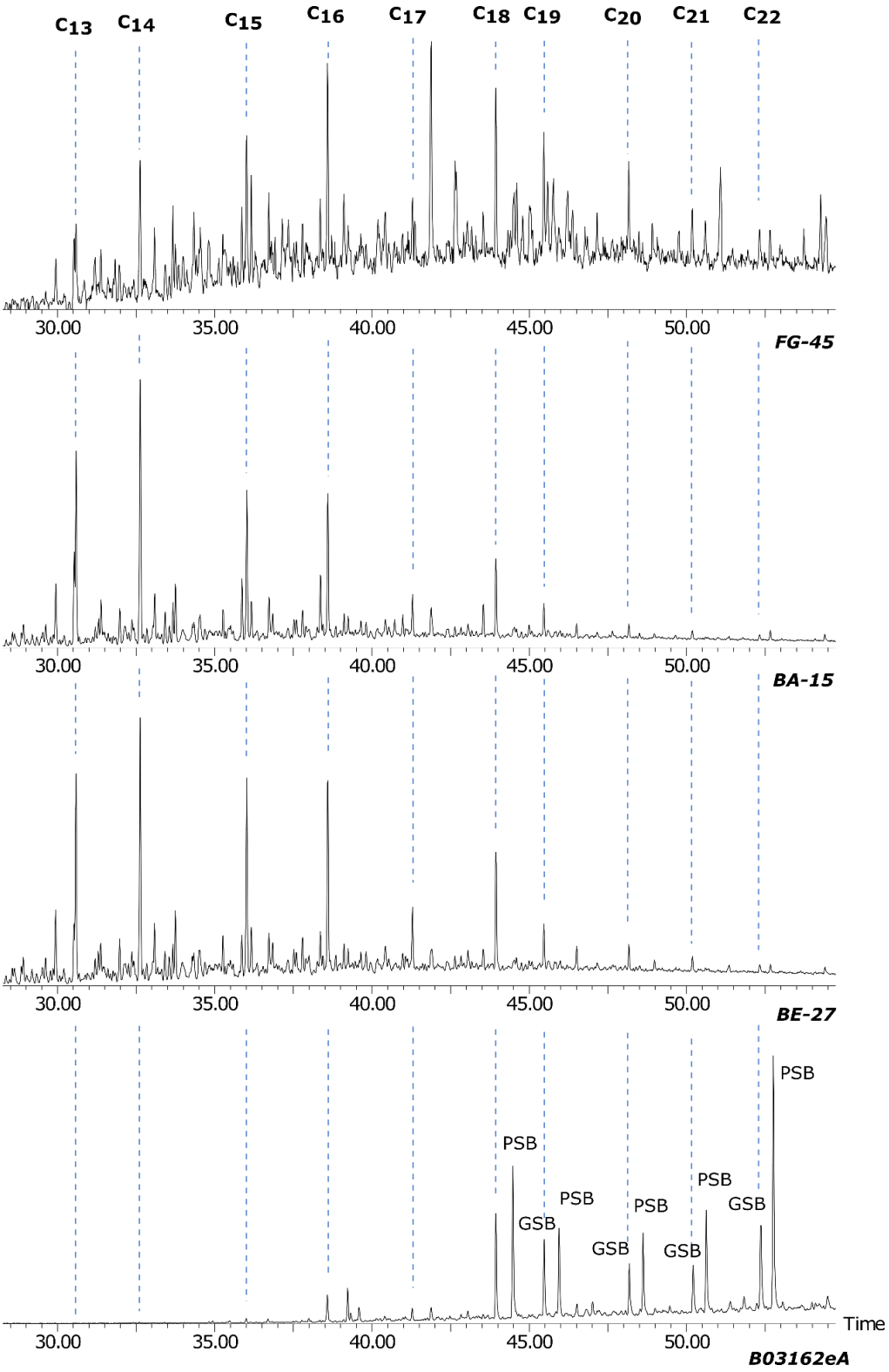

Figure S-2 M/z 134 partial ion chromatograms from the aromatic hydrocarbon fractions. Sample B03162eA (Brocks *et al.*, 2005) was used to identify 2,3,6-trimethyl aryl isoprenoid peak positions.

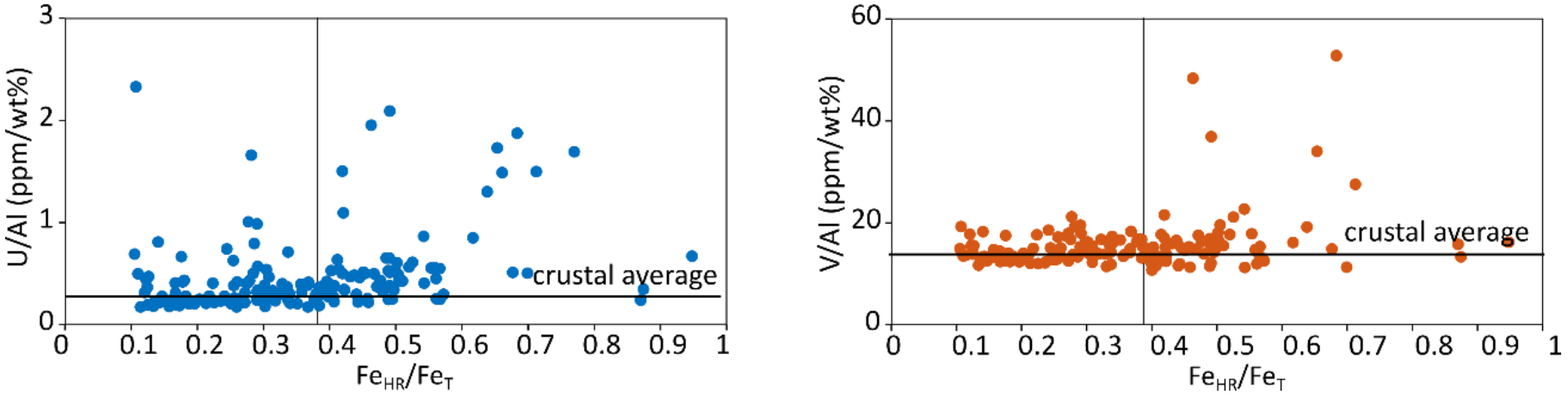

Figure S-3 U/Al and V/Al *versus* Fe_{HR}/Fe_T ratios. The vertical line represent the 0.38 threshold between oxic (<0.38) and anoxic (>0.38) environments (Canfield *et al.*, 2008). The horizontal lines represent the crustal averages (Rudnick and Gao, 2003).

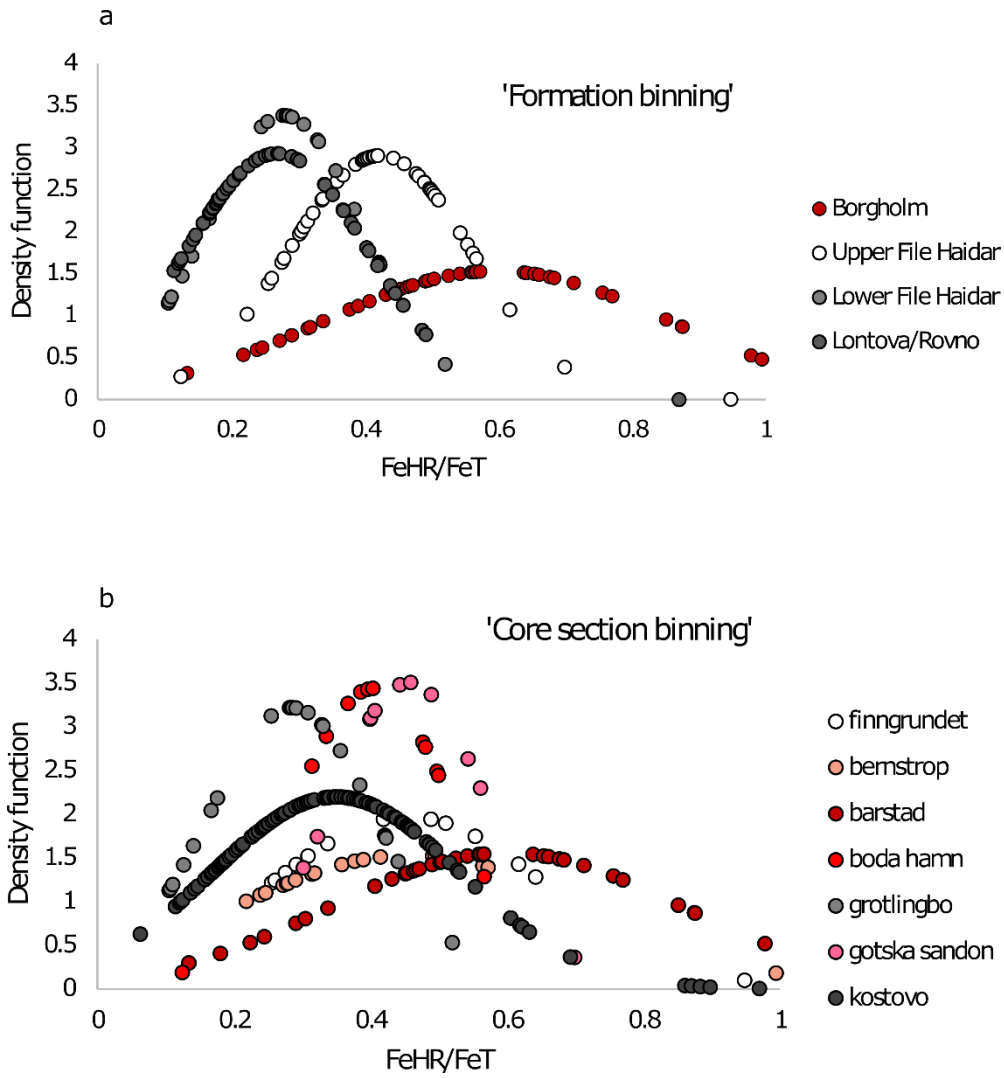

Figure S-4 Alternative binning strategies of the redox data, **(a)** using geological formations as a discriminant and **(b)** using core sections as a discriminant. Our preferred strategy was adopted in Figure 3, using stratigraphic sequencing, because both 'formation-binning' and 'core-section-binning' methods are too coarse to account for the large spatial variability within either terms (formations or sections). Nevertheless, the two alternatives point towards a similar trend in redox data distribution, with denser occurrences of anoxic data in mid-shelf settings, and denser occurrences of oxic data in shallower and deeper sediments.

Supplementary Information References

Bergström, J., Ahlberg, P. (1981) Uppermost Lower Cambrian biostratigraphy in Scania, Sweden. *GFF* 103, 193–214.

Boreham, C., Crick, I., Powell, T. (1988) Alternative calibration of the Methylphenanthrene Index against vitrinite reflectance: Application to maturity measurements on oils and sediments. *Organic Geochemistry* 12, 289–294.

Brocks, J.J., Schaeffer, P. (2008) Okenane, a biomarker for purple sulfur bacteria (Chromatiaceae), and other new carotenoid derivatives from the 1640Ma Barney Creek Formation. *Geochimica et Cosmochimica Acta* 72, 1396–1414.

Brocks, J.J., Love, G.D., Summons, R.E., Knoll, A.H., Logan, G.A., Bowden, S.A. (2005) Biomarker evidence for green and purple sulphur bacteria in a stratified Palaeoproterozoic sea. *Nature* 437, 866–870.

Brocks, J.J., Grosjean, E., Logan, G.A. (2008) Assessing biomarker syngeneity using branched alkanes with quaternary carbon (BAQCs) and other plastic contaminants. *Geochimica et Cosmochimica Acta* 72, 871–888.

Butterfield, N.J. (1994) Burgess Shale-type fossils from a Lower Cambrian shallow-shelf sequence in northwestern Canada. *Nature* 369, 477–479.

Canfield, D.E., Raiswell, R., Westrich, J.T., Reaves, C.M., Berner, R.A. (1986) The use of chromium reduction in the analysis of reduced inorganic sulfur in sediments and shales. *Chemical Geology* 54, 149–155.

Canfield, D.E., Poulton, S.W., Knoll, A.H., Narbonne, G.M., Ross, G., Goldberg, T., Strauss, H. (2008) Ferruginous Conditions Dominated Later Neoproterozoic Deep-Water Chemistry. *Science* 321, 949–952.

Hagenfeldt, S.E. (1989a) Lower Cambrian acritarchs from the Baltic Depression and south-central Sweden, taxonomy and biostratigraphy. *Stockholm Contributions in Geology* 41, 1–176.

Hagenfeldt, S.E. (1989b) Middle Cambrian acritarchs from the Baltic Depression and south-central Sweden, taxonomy and biostratigraphy. *Stockholm Contributions in Geology* 41, 177–250.

Hagenfeldt, S.E. (1994) The Cambrian File Haidar and Borgholm Formations in the central Baltic and south central Sweden. *Stockholm Contributions in Geology* 43, 69–110.

Hagenfeldt, S., Bjerkéus, M. (1991) Cambrian acritarch stratigraphy in the central Baltic Sea, Sweden. *GFF* 113, 83–84.

Jarrett, A.J., Schinteie, R., Hope, J.M., Brocks, J.J. (2013) Micro-ablation, a new technique to remove drilling fluids and other contaminants from fragmented and fissile rock material. *Organic Geochemistry* 61, 57–65.

Jensen, S. (1997) *Trace fossils from the Lower Cambrian Mickwitzia sandstone, south-central Sweden*. Scandinavian University Press, Oslo.

Kirschvink, J.L., Ripperdan, R.L., Evans, D.A. (1997) Evidence for a large-scale reorganization of Early Cambrian continental masses by inertial interchange true polar wander. *Science* 277, 541–545.

Kirsimäe, K., Jørgensen, P., Kalm, V. (1999) Low-temperature diagenetic illite-smectite in Lower Cambrian clays in North Estonia. *Clay Minerals* 34, 151–151.

Koopmans, M.P., Schouten, S., Kohnen, M.E., Damsté, J.S.S. (1996) Restricted utility of aryl isoprenoids as indicators for photic zone anoxia. *Geochimica et Cosmochimica Acta* 60, 4873–4876.

Lyons, T.W., Reinhard, C.T., Planavsky, N.J. (2014) The rise of oxygen in Earth/'s early ocean and atmosphere. *Nature* 506, 307–315.

McManus, J., Berelson, W.M., Klinkhammer, G.P., Hammond, D.E., Holm, C. (2005) Authigenic uranium: Relationship to oxygen penetration depth and organic carbon rain. *Geochimica et Cosmochimica Acta* 69, 95–108.

McManus, J., Berelson, W.M., Severmann, S., Poulson, R.L., Hammond, D.E., Klinkhammer, G.P., Holm, C. (2006) Molybdenum and uranium geochemistry in continental margin sediments: Paleoproxy potential. *Geochimica et Cosmochimica Acta* 70, 4643–4662.

Nielsen, A.T., Schovsbo, N.H. (2011) The Lower Cambrian of Scandinavia: depositional environment, sequence stratigraphy and palaeogeography. *Earth-Science Reviews* 107, 207–310.

Nielsen, A.T., Schovsbo, N.H. (2015) The regressive Early-Mid Cambrian 'Hawke Bay Event' in Baltoscandia: Epeirogenic uplift in concert with eustasy. *Earth-Science Reviews* 151, 288–350.

Och, L.M., Shields-Zhou, G.A. (2012) The Neoproterozoic oxygenation event: environmental perturbations and biogeochemical cycling. *Earth-Science Reviews* 110, 26–57.

Partin, C.A., Bekker, A., Planavsky, N.J., Scott, C.T., Gill, B.C., Li, C., Podkovyrov, V., Maslov, A., Konhauser, K.O., Lalonde, S.V., Love, G.D., Poulton, S.W., Lyons, T.W. (2013) Large-scale fluctuations in Precambrian atmospheric and oceanic oxygen levels from the record of U in shales. *Earth and Planetary Science Letters* 369–370, 284–293.

Peters, K.E., Walters, C.C., Moldowan, J.M. (2005) *The biomarker guide*. Cambridge University Press, Cambridge.

Poulton, S.W., Canfield, D.E. (2005) Development of a sequential extraction procedure for iron: implications for iron partitioning in continentally derived particulates. *Chemical Geology* 214, 209–221.

Rudnick, R., Gao, S. (2003) Composition of the continental crust. *Treatise on Geochemistry* 3, 1–64.

Schovsbo, N.H. (2001) Why barren intervals? A taphonomic case study of the Scandinavian Alum Shale and its faunas. *Lethaia* 34, 271–285.

Schwark, L., Frimmel, A. (2004) Chemostratigraphy of the Posidonia Black Shale, SW-Germany: II. Assessment of extent and persistence of photic-zone anoxia using aryl isoprenoid distributions. *Chemical Geology* 206, 231–248.

Slater, B.J., Harvey, T.H.P., Guilbaud, R., Butterfield, N.J. (2017) A cryptic record of Burgess Shale-type diversity from the early Cambrian of Baltica. *Palaeontology* 60, 117–140.

Summons, R., Powell, T. (1987) Identification of aryl isoprenoids in source rocks and crude oils: biological markers for the green sulphur bacteria. *Geochimica et Cosmochimica Acta* 51, 557–566.

Thickpenny, A. (1984) The sedimentology of the Swedish alum shales. *Geological Society, London, Special Publications* 15, 511–525.

Zhang, S., Wang, X., Wang, H., Bjerrum, C.J., Hammarlund, E.U., Costa, M.M, Connelly, J.N., Zhang, B., Su, J., Canfield, D.E. (2016) Sufficient oxygen for animal respiration 1,400 million years ago. *Proceedings of the National Academy of Sciences* 113, 1731–1736.